First Optical Measurement of ^{55}Fe Spectrum in a TPC

N. S. Phan[1], R. J. Lauer, E. R. Lee, D. Loomba, J. A. J. Matthews, E. H. Miller

Department of Physics and Astronomy, University of New Mexico, NM 87131, USA

Abstract

The first energy spectrum from an ^{55}Fe X-ray source obtained by a TPC with an optical imaging device is presented. The low pressure gaseous TPC is operated with GEM/THGEM amplification and read out with a fast lens and low noise CCD optical system. Effective gas gains of greater than 2×10^6 were obtained over a pressure range of 35-100 Torr in pure carbon tetrafluoride (CF_4) gas. The high signal-to-noise detector allowed individual ionization tracks from X-ray interactions to be imaged and resolved. This would additionally allow for detector spatial gain uniformity to be mapped out as well as push lower discrimination threshold in some rare event searches such as dark matter detection.

Keywords: Optical TPC, ^{55}Fe, GEMs, Thick GEMs, CF_4, CCD, electronic recoil

1. Introduction

The capability of a high resolution and high signal to noise detector useful for studies of low energy recoils is demonstrated. We show that with sufficient gas gain and light collection efficiency, the tracks produced by 5.9 keV ^{55}Fe X-rays can be imaged optically by a low-noise, high quantum efficiency CCD (charge-coupled device) camera. This is to our knowledge the first time that an ^{55}Fe spectrum has been acquired with an optical imaging device. To accomplish this, we used a low pressure TPC (time projection chamber) operated over a range of 35-100 Torr in CF_4 with GEM (gas electron multiplier) and thick GEM (THGEM) amplification and CCD camera

---

[1]Corresponding author

readout. GEMs are a micro-pattern amplification device invented by Sauli at the European Organization for Nuclear Research (CERN) [1], and further information on the operation of GEMs with CCD readout can be found in Refs. [2, 3, 4]. THGEMs are very similar to GEMs but with dimensions (thickness, hole size, and pitch) that are typically about one order of magnitude larger, and exceptionally high gas gains have been achieved in both types of amplification devices over a wide range of pressures [5, 6].

The operating principle of our detector is as follows: A particle creates an ionization track in the detection volume. The ionization drift towards the GEM/THGEM amplification device due to an electric field between the cathode and opposing GEM/THGEM surface. Upon arriving at the amplification device, the ionization is channeled into the GEM/THGEM holes where a strong dipole electric field is established through a potential difference between the top and bottom surfaces of device. Once inside this strong field region, electrons are multiplied by collisional avalanche, a process that also creates scintillation light in some gases such as CF_4. In a multi-GEM/THGEM arrangement, the ionization then drifts onto the next GEM/THGEM stage and is amplified once more until it arrives at the last stage. Once there, the charges are amplified for the last time, and the scintillation light is imaged by a low-noise CCD camera and a fast lens setup looking down on the surface of the final amplification stage.

2. Detector Setup

The detector setup and amplification device is shown in Figure 1. At each pressure, the choice of amplification device (single GEM/THGEM or multiple GEM/THGEM) is made to maximize stability, gas gain, and spatial resolution. For the 100 Torr measurement, the detector consists of three standard copper GEMs (Gaseous Electron Multipliers) arranged in a cascade with 2 mm separation between them (Figure 1). The GEMs are manufactured at CERN and consist of a 50 μm thick sheet of kapton with an area of 7×7 cm^2. The sheet is cladded with coper on both surfaces and mounted on G10 frames. The GEM surface is chemically etched with a hexagonal array of bi-conical holes of diameter of 50/70 μm (inner/outer) and at a pitch of 140 μm. For a thorough review of GEMs, see Ref. [7]. Below the GEMs sits a 7×7 cm^2, ~ 360 μm thick copper cathode mesh with ~ 500 μm pitch. Together the surface of the cathode and the nearest GEM surface form a 1 cm detection volume (drift volume). Finally, situated 3 mm above the top
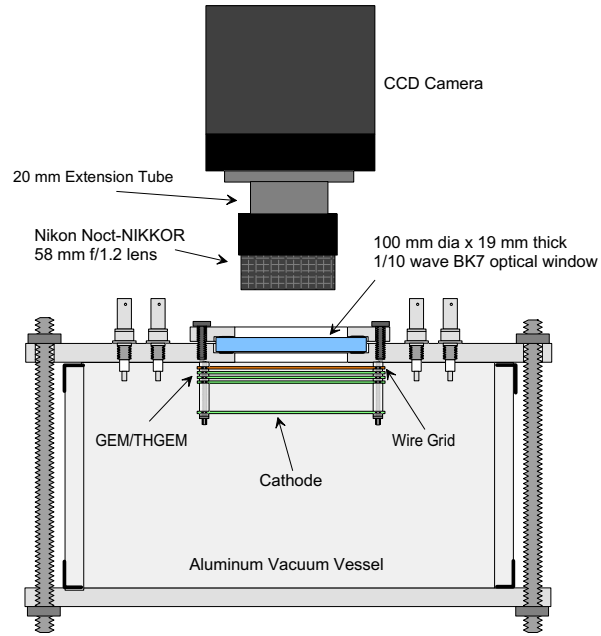
(a) Detector Vessel
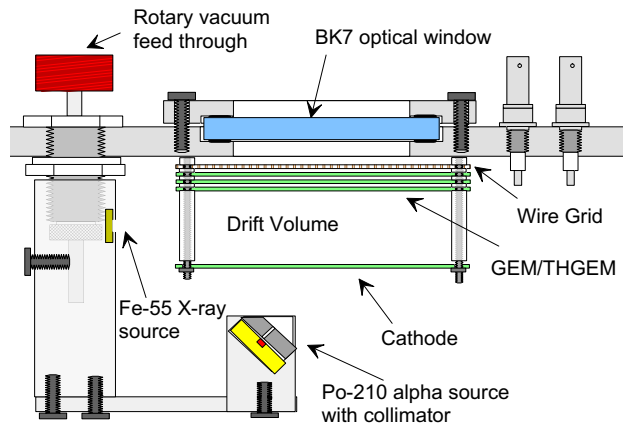
(b) Detection Volume

Figure 1: (a) A simplified drawing of the CCD detector showing the aluminum vacuum vessel and CCD camera setup, excluding the rotary feedthrough, camera mount, and calibration sources for clarity. The light box is also excluded to show the lens and extension tube. (b) A close up view of the detection volume, showing the locations of the calibration sources, cathode, wire grid, and GEMs/THGEMs.

most GEM (GEM 3) is a 1 mm pitch anode wire grid plane made from 20 μm thick gold plated tungsten wires, forming the induction gap.

At 50 Torr, the standard CERN GEMs are replaced by a single copper coated thick GEM (THGEM) [REF]. We observe that GEMs appear unsuited for high gain operation in lower pressure. For instance in 75 Torr, the maximum stable gas gain was insufficient for imaging ^{55}Fe tracks. The THGEM is made from a 0.4 mm thick PCB with $\sim$ 0.3 mm holes mechanically drilled over a 3×3 cm^2 copper coated area. The holes have a pitch of 0.5 mm, and due to the lower pressure of operation and the longer ranges of tracks, the drift gap is increased from 1 cm to 2 cm. In addition, the separation from the amplification device and the wire grid is increased from 3 mm to $\sim$ 7 mm.

In the 35 Torr measurements, two THGEMs with a 9.5×9.5 cm^2 active area (avalanche area) are used for the amplification stage. These THGEMs have the same hole size, thickness, and pitch as the one used in the 50 Torr measurements. The drift gap, transfer gap between the THGEMs, and induction gap between the THGEM and wire grid are 2 cm, 4 mm, and 9.5 mm, respectively. In addition, the wire grid size is increased to match the THGEM area by laying copper tape around the perimeter of the wire frame.

For all pressure measurements, the detector is housed inside an $\sim$ 10 liter cylindrical aluminum vacuum vessel. Calibration is done using internally mounted ^{55}Fe (5.9 keV X-rays) and ^{210}Po (5.3 MeV alphas) sources, which can be individually turned on or off using a rotary feedthrough (Figure 1b). Prior to powering up the GEMs/THGEMs, the vacuum vessel is pumped down over at least one day to $<$ 0.1 Torr and back-filled with pure (99.999%) carbon tetrafluoride (CF$_4$) gas. A 4-inch diameter BK-7 glass window is positioned above the wire grid to allow scintillation light from the final amplification stage to be captured by the CCD camera. BK-7 is a material with a relatively high transmittance for the optical component of the CF$_4$ scintillation, which peaks around 620 nm [8, 9], and is relatively cost-efficient as compared to quartz.

Track images are captured with a fast 58 mm f/1.2 Nikon Noct-NIKKOR lens mated to a back-illuminated Finger Lakes Instrumentation (FLI) CCD camera (MicroLine ML4710-1-MB) through a 20 mm extension tube for close-focusing imaging. The whole setup is mounted on top of the vacuum vessel (Figure 1a) in a light tight box. The camera contains an E2V made 18.8 mm diagonal sensor with a 1024×1024 pixel array (CCD47-10-1-353), each pixel with a size of 13×13 μm^2. The mid-band coated CCD sensor has a peak

quantum efficiency of 96% at 560 nm and can be cooled down to a stable operating temperature of $-38°$C using the built-in Peltier cooler at ambient room temperature. Two readout speeds are available, 700 kHz and 2 Mhz, with 16-bit digitization and maximum 16×16 on-chip pixel binning. At the lowest operating temperature and slowest readout mode, the read-out noise is ~ 10 e^- rms and the dark current is ~ 0.03 e^-/pix/sec at 1×1 on-chip pixel binning. At our focusing distance, the CCD-lens system images $\sim 3 \times 3$ cm^2 region of the GEM/THGEM surface. The known pitch of the holes on this surface is used to calibrate the length-scale of the images.

3. Detector Calibrations

3.1. GEM/THGEM Gain

The gain was determined by use of an ORTEC 448 research pulse generator and an ORTEC 142IH charge sensitive preamplifier which read out the charge signal from the last GEM/THGEM surface rather than the wire grid. The pulse generator output was connected to the test input of the preamplifier which has a built-in 1 pF capacitor for calibration purposes. This allowed the preamplifier gain (fC/V) to be determined. An ^{55}Fe 5.9 keV X-ray source is then used to determine the effective gas gain from the output voltage signal of the preamplifier. The X-ray source creates on average 172 electron-ion pairs per conversion event which was calculated from the W-value (the average energy per ionization) of 34.2 eV for CF$_4$ [10].

At a pressure of 100 Torr, the maximum stable effective gas gain of $\sim 1 \times 10^5$ was achieved with GEM 1 = 279 V, GEM 2 = 334 V, and GEM 3 = 380 V, drift field of 400 V/cm, transfer fields of 1.40 kV/cm and 1.67 kV/cm between GEMs 1 and 2 and GEMs 2 and 3, respectively, and induction field of 260 V/cm between GEM 3 and the grid. The test for stability was done by firing a highly ionizing source (^{210}Po alpha source) into the detection volume. If no sparks occur over several hours, then the voltage setting is deemed stable. A higher effective gas gain of $\sim 2 \times 10^5$ was achieved with GEMs 1 and 2 = 290 V and GEM 3 = 450 V. The drift, transfer, and induction fields were 400 V/cm, 1.45 kV/cm, and 360 V/cm, respectively. This setting, however, was not entirely stable under alpha irradiation and initiated a spark about once per hour. Nevertheless, we were able to acquired ^{55}Fe images and an energy spectrum at this setting.

For the 50 Torr measurements, the THGEM was powered to a voltage of 830 V and the drift field was set to 200 V/cm. The induction field was 824

V/cm with the wire grid at a lower voltage than the top THGEM surface so that all electrons produced in the avalanche were collected by this electrode. The electrical stability at this voltage setting was similar to the highest gain setting at 100 Torr in that both were moderately but not completely stable. No gas gain measurements were made but we estimate the gain to be $\sim 1.5 \times 10^5$ based on the oscilloscope amplitude of the ^{55}Fe signals.

Finally, in the 30 Torr measurements, the THGEM voltage biases were THGEM 1 = 573 V and THGEM 2 = 470 V, where THGEM 1 is the one facing the cathode and THGEM 2 is the THGEM nearest to the wire grid. The drift, transfer, and induction fields were 200 V/cm, 718 V/cm, and 495 V/cm, respectively. No precise gain measurements were made at this voltage setting, but an estimate of the effective gain made by using the preamplifier gain (fC/V) determined previously and the amplitude of the ^{55}Fe signals on the oscilloscope gives an approximate value of 1.6×10^5.

3.2. CCD Calibration

The CCD images (or frames) were calibrated using a set of co-averaged flat-field and dark frames. Dark frames, which are typically taken with the same exposure time as the image frame but with the camera shutter closed, are used to correct for the variable accumulation rate of dark current across pixels. Flat-field frames, on the other hand, are acquired by taking exposures of a uniformly illuminated screen. This allowed for correcting of vignetting and pixel to pixel variation in light sensitivity. For each type of calibration frame, a set of such frames were co-averaged together to create what are usually referred to as a master calibration frame. The averaging was done with an algorithm that rejected cosmic rays and radioactivity hit pixels by comparing the value of the same pixel across the set of frames and excluding those above three sigmas of the initial average of the pixels. The average is then re-computed and the process was repeated until there was a convergence in the average value of the pixels. Finally, the calibration was done by subtracting the master dark frame from each image frame and then dividing the resulting frame by the normalized, master flat-field calibration frame.

4. Results

4.1. 100 Torr

The energy spectrum was obtained by imaging a set of electronic recoils from ^{55}Fe X-ray interactions in the gas. A spectrum taken at the maximum
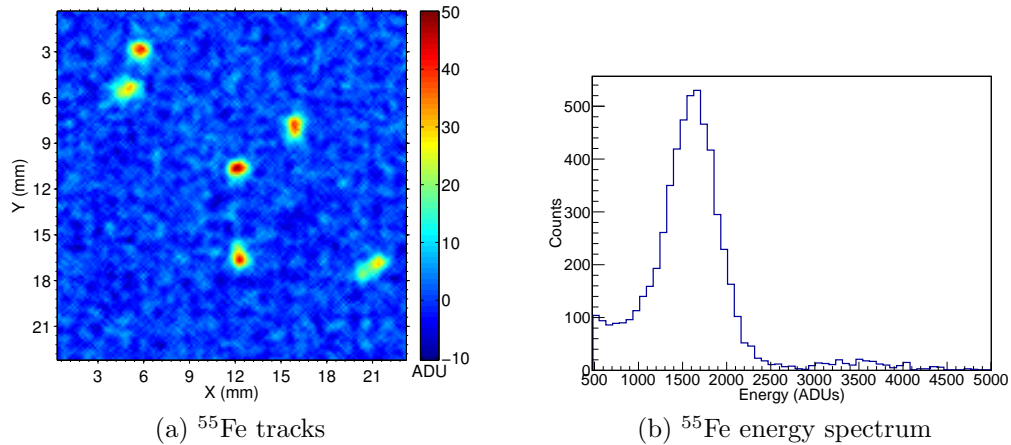
(a) ^{55}Fe tracks

(b) ^{55}Fe energy spectrum

Figure 2: (a) An image of ^{55}Fe tracks acquired at 6×6 on-chip binning in 100 Torr CF_4 with an averaging filter of block size 5×5 applied to the image to enhance signal-to-noise. The image is captured at the maximum stable gas gain of $\sim 10^5$ and has a pixel scale of 165 μm/pix. (b) An energy spectrum of ^{55}Fe obtained optically from CCD imaging of electronic recoil tracks at 6×6 on-chip binning and the maximum stable gain. The data is a combination of the start and end data sets in the day eight run (see Figure 4). The smaller secondary feature to the right of the primary peak is the result of event pile-up.

stable gain setting in 100 Torr CF_4 is shown in Figure 2b in units of ADUs (analog to digital units). One ADU corresponds to about 1.3 e^- produced in the CCD sensor. A sample image containing ^{55}Fe tracks taken in 100 Torr CF_4 and at the maximum stable setting with 6×6 binning is shown in Figure 2a. The signal-to-noise and resolution are high enough that individual tracks are resolved well above the noise in the CCD image. Additionally, the spatial uniformity of the gas gain can be easily characterized with this level of signal-to-noise and resolution.

The peak value in the energy spectrum in Figure 2b is obtained from a fit which comprises of a single Gaussian signal component and uniform and exponential background components. The range of the fit is set so as to exclude the secondary peak due to pile-up events. The fit has a reduced χ^2 (χ^2/ndf) = 0.66, a peak value of $\mu_{100\text{Torr}} = 1621 \pm 5$, and $\sigma_{100\text{Torr}} = 264 \pm 5$. The FWHM energy resolution is 38% and an energy conversion factor of 275 ADUs/keV.

In Figures 3a and 3b, a sample image of ^{55}Fe tracks imaged in 100 Torr CF_4 at a gain $\sim 2 \times 10^5$ is shown along with the corresponding energy spectrum. The same procedure for fitting the spectrum as described above
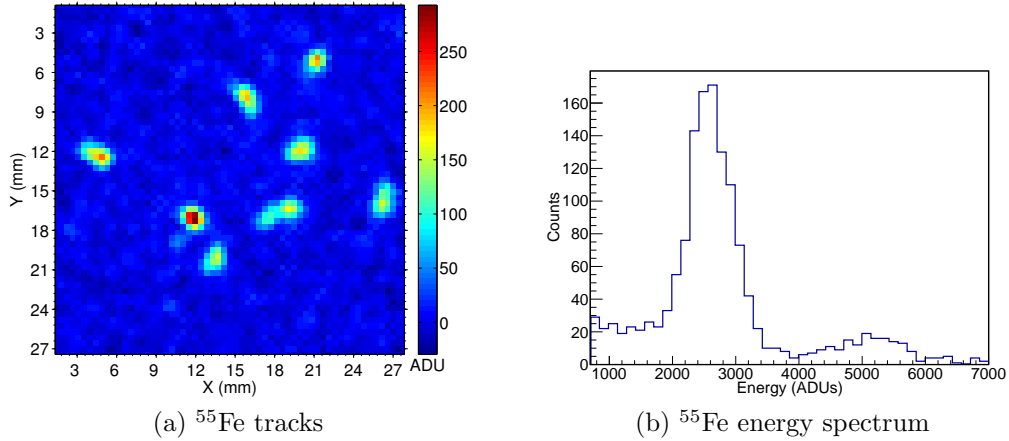
(a) ^{55}Fe tracks   (b) ^{55}Fe energy spectrum

Figure 3: (a) An image of ^{55}Fe tracks acquired at 16×16 on-chip binning (pixel scale of 440 μm/pix) in 100 Torr CF_4 with an averaging filter of block size 3×3 applied to the image to enhance signal-to-noise. The image is captured at the maximum gas gain of $\sim 2 \times 10^5$ and shows that even in 100 Torr, ^{55}Fe tracks are resolved. (b) An ^{55}Fe energy spectrum obtained optically from CCD imaging of electronic recoil tracks at 16×16 on-chip binning and maximum gain of $\sim 2 \times 10^5$. The smaller secondary feature to the right of the primary peak is due to event pile-up.

gives a peak value of 2610 ± 15, σ of 329 ± 16, and energy conversion factor of 443 ADUs/keV. Interestingly, the FWHM energy resolution implied from the fit is 30%, significantly smaller than the resolution of the moderate gain 100 Torr data. A possible explanation for the this is that the higher ΔV of GEM 3 and the resulting higher electric field inside the GEM holes could decrease the probability for electron attachment in this region and help minimize the degradation of energy resolution.

4.2. Light Quenching

Another interesting feature is the apparent difference in the ratio of spectrum peak to the corresponding effective gas gain for the two 100 Torr data sets. In the moderate but stable gain data, the ratio is ~ 0.016, and in the high gain data, the ratio is ~ 0.013. This ratio could be thought of as an effective photon yield and implies that the high gain data has a photon yield that is approximately 19% lower than the moderate gain data. This observation could be explained as a decrease in the photon yield with increasing charge density at high gas gains so that the total number of photons emitted for every secondary electron created in the avalanche region is reduced. How-
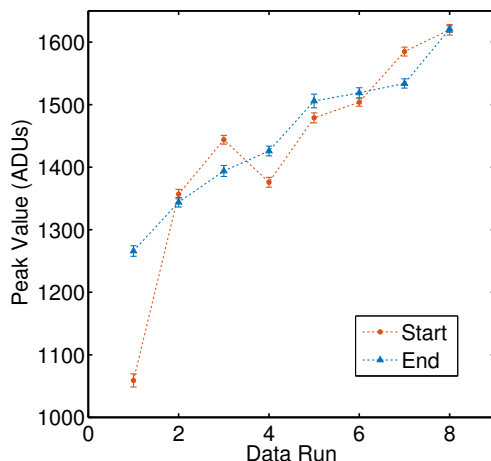
8

Figure 4: The fitted peak value of the ^{55}Fe energy spectrum at the start and end of the day over eight days of data taking. With the exception of the first data run, the start and end peak values are within 4%. The large change ($\sim 20\%$) seen between the start and end in the first data set is likely due to insufficient time for the GEMs to charge up and stabilize. The raising peak value with run number is likely the result of a reduction in concentration of contaminants with the additional pump down in-between runs.

ever, it could also be possible that the emission spectrum from CF_4 changes with the gas gain so that the number of photons produced in the wavelength range of sensitivity for the CCD camera and lens is reduced.

The simplest explanation, however, is the presence of light output suppressing contaminants in the gas. This possibility is explored by comparing data from many ^{55}Fe imaging sequences for the moderate gain but stable voltage setting. In total eight days of data were taken with a set of images acquired at the beginning and end of the day for a total of 16 data sets. In-between the two ^{55}Fe imaging sequences for each day, a neutron data sequence was conducted. The results of those data are presented elsewhere. At the end of each day of data taking which lasts about 16 hours each, the vessel was pumped down for 2-3 hours and back-filled with fresh gas, so that the last day in the sequence (day 8) should have the highest gas purity. Throughout the 8 days, the vessel was sealed and no changes were made to the experimental setup other the pump down and gas back-filling at the start of each day. For each imaging sequence, approximately two hours of ^{55}Fe imaging data was acquired, and all data sets were analyzed identically.

The results of the data runs are plotted in Figure 4 which shows the

9

fitted peak value for the start and end of each day of data acquisition. The large difference in the start and end spectrum peak values for data run 1 is most likely the result of insufficient time for the GEM to charge up and reach a stable operational state. With the exception of run 1, the start and end spectrum peak values are always within 4% of each other which suggests that out-gassing from detector surfaces and components and compositional change from avalanche over a single day does not cause the light output to change significantly over the same time period. This is not to say that out-gassing does not effect the light output at all. A clear rising trend is seen in the spectrum peak value with the data runs. The light output increases by 28% between run 1 and run 8 in the end series and by 53% between run 1 and run 8 in the start series. The end series is monotonically increasing whereas the start series has an inflection which indicates that the GEM charge up time is important. The differences in peak values between runs 1 and 8 in both series could completely explain the 19% photon yield difference between the high gain and moderate gain data sets. The ratio of peak value to gas gain for end-run 1 is 0.013 which is the same value as that for the high gain data set. Nevertheless, we cannot entirely rule out other effects such as a charge density dependent photon yield or a charge up time effect. Finally, there is also a question of how long the pump down time must be because Figure 4 shows that the light output is still increasing even after day 8.

Light output quenching resulting from gas contamination could be dealt with with a long pump down and/or continuous filtering of the gas in a circulation system. However, quenching due to high charge density arising from either high gas gains and/or high primary ionization densities raises several interesting and important questions. Is the charge quenched or saturated by a similar amount to the light, so the the charge to light ratio is the same in the quenched region as it is in the unquenched region? How does the onset of quenching change with the type of the gas and pressure/density? Finally, does the quenching behavior change when different amplification devices are used? In other words, if all operating parameters (i.e. gas, pressure, gain, etc.) are the same, does the effect differ when multi-wire proportional chambers (MWPCs) are used rather than GEMs or THGEMs?

It may be crucial to answer these questions particularly in regards to directional dark matter detection in which the sense (vector direction) of the ionization track is determined by measuring the asymmetry in the charge deposition along the track. If quenching plays a significant role in the low pressure regime that directional dark matter experiments operate in, this can
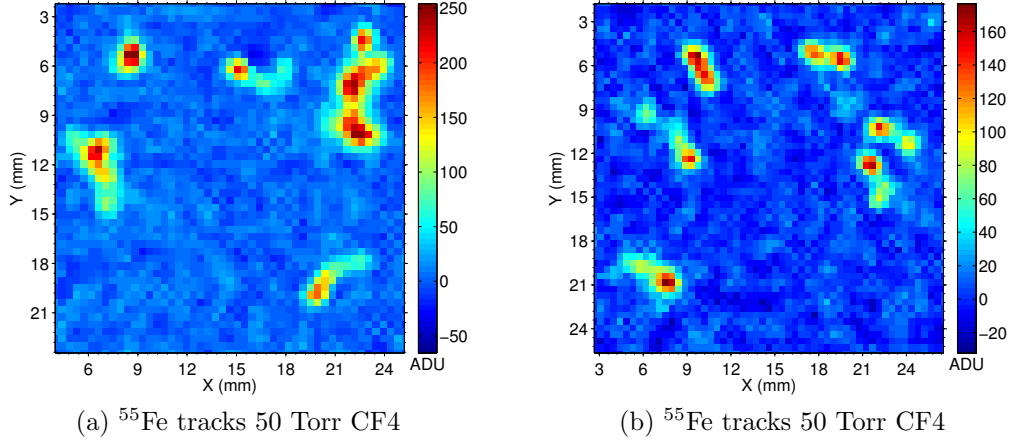
(a) ^{55}Fe tracks 50 Torr CF4   (b) ^{55}Fe tracks 50 Torr CF4

Figure 5: (a)-(b) Images of 5.9 keV ^{55}Fe electronic recoil tracks in 50 Torr CF4 at 16×16 on-chip binning. An averaging filter with a 3×3 block size has been applied to the image to improve signal-to-noise without significantly degrading resolution. At this pressure, the tracks are well resolved and fluctuations in energy loss and range straggling are also clearly seen.

place a constraint on how well the directional signature can be measured in gas based TPCs operated at high gas gains.

4.3. 35 & 50 Torr

In Figure 5, two sample images of ^{55}Fe tracks taken at a pressure of 50 Torr in CF$_4$ are shown. The tracks are much better resolved than those in the 100 Torr data, and additionally, differences in ionization density are also clearly visible. The corresponding energy spectrum is not shown because not enough images were taken at this pressure due to an issue with electrical stability. Nevertheless, these images show unambiguously that electron recoils with energies as low as 5.9 keV are still resolvable given sufficient detector signal-to-noise and imaging resolution. This is an important topic in rare event searches such as directional dark matter experiments where discrimination between electronic and nuclear recoils is of great interest.

For the 35 Torr data, a sample image containing ^{55}Fe tracks is shown in Figure 6a. The tracks are clearly resolvable but resolution is not quite as good as the 50 Torr data due to the 0.5 mm pitch of the double THGEM amplification structure and the transfer region in-between the two. The energy spectrum obtained from taken a series of these images is shown in
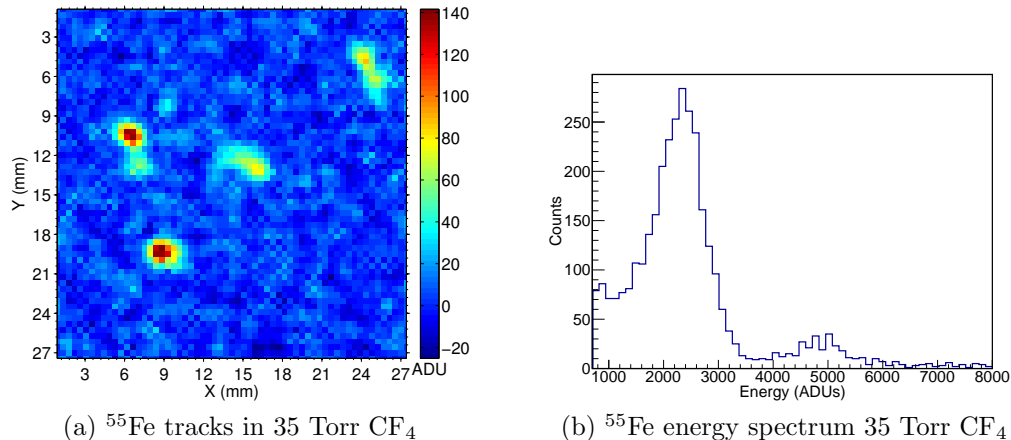
11

(a) ^{55}Fe tracks in 35 Torr CF$_4$ (b) ^{55}Fe energy spectrum 35 Torr CF$_4$

Figure 6: (a) An image of ^{55}Fe tracks in 35 Torr CF$_4$ with an averaging filter applied to enhance signal to noise. The tracks are clearly resolvable as extended objects rather than diffused points at this pressure. (b) An energy spectrum obtained from CCD imaged ^{55}Fe electronic recoil tracks in 35 Torr at 16×16 on-chip binning and maximum stable gain. The smaller secondary feature on the right of the primary peak is due to event pile-up.

Figure 6b. A fit of the spectrum to a single Gaussian signal component and a background component which consists of a uniform and exponential components gives a reduced χ^2 $(\chi^2/ndf) = 0.80$. The fitted peak value is $\mu_{35\text{Torr}} = 2327 \pm 18$ and $\sigma_{35\text{Torr}} = 400 \pm 28$. This gives a FWHM energy resolution of 40% which is similar to within errors to the the energy resolution obtained from the moderate gain 100 Torr data but is not as good as the high gain data at the same pressure.

5. Conclusion

We have shown that a GEM and THGEM based detector can be operated in low pressure CF$_4$ (35-100 Torr) with gains exceeding 2×10^5. This allowed individual ^{55}Fe tracks to be imaged by a low noise CCD camera and for an optically measured spectrum to be obtained for the first time. We found that it is important to pump down the detector for an extended period of time to reduce contaminants in the gas that can suppress light output. However, it is not clear if light quenching at high charge densities is a significant effect for experiments that use the asymmetry in charge density to determine the recoil direction of a track. Finally, we showed that electronic recoils as low as 5.9 keV in energy can be resolved. This is important for rare event searches

12

such as direct dark matter detection experiments that rely on differences in stopping power to discriminate between different types of recoils.

Acknowledgements

[1] F. Sauli, Nucl. Instr. and Meth. Phys. Res. A, 1997, vol. 386, p. 531.

[2] F. A. F. Fraga et al., Nucl. Instr. and Meth. Phys. Res. A 471 (2001) 125130.

[3] F. A. F. Fraga et al., Nucl. Instr. and Meth. Phys. Res. A 478 (2002) 357361.

[4] F. A. F. Fraga et al., Nucl. Instr. and Meth. Phys. Res. A 513 (2003) 379387.

[5] C. Shalem, R. Chechik, A. Breskin, K. Michaeli, Nucl. Instr. Meth. A 558 (2006) 475489.

[6] C.K. Shalem, R. Chechik, A. Breskin, K. Michaeli, N. Ben-Haim, Nucl. Instr. Meth. A 558 (2006) 468474.

[7] A. F. Buzulutskov, Instr. Exp. Tech., 2007, Vol. 50, No. 3, pp. 287.

[8] A. Morozov, M. M. F. R. Fraga, L. Pereira, L. M. S. Margato, S. T. G. Fetal, B. Guerard, G. Manzin, F. A. F. Fraga, Nucl. Instr. Meth. Phys. Res. B 268 (2010) 14561459.

[9] A. Kaboth, et al., Nucl. Instr. and Meth. A 592 (2008) 63.

[10] G.F. Reinking, L. G. Christophorou, and S. R. Hunter, J. Appl. Phys. 60, 499 (1986).